Superconducting gap symmetries in $YBa_2Cu_3O_{7-\delta}$ compatible with electronic Raman efficiencies and the local-density-approximation band structure

Matthias Krantz
Max-Planck-Institut für Festkörperforschung, Heisenbergstrasse 1, D-70569 Stuttgart, Federal Republic of Germany
(Received 9 February 1996)

Superconductivity induced absolute electronic Raman efficiencies are presented for single-domain $YBa_2Cu_3O_{7-\delta}$ in *a-b* plane polarization geometries and compared with spectra calculated from gauge invariant theory using realistic Raman vertices derived from the local-density-approximation band structure. Effective mass fluctuations, screening, gap size, and anisotropy on the multisheeted Fermi surface are systematically investigated. It is argued that the observed anisotropy of the A_{1g}, B_{2g}, and B_{1g} spectra requires two different gaps on the CuO_2 plane Fermi surfaces of *even* and *odd* parity. Respective time reversal invariant gaps of B_{1g} and A_{1g} symmetry (e.g., $\Delta_{\rm even}=d_{x^2-y^2}$, $\Delta_{\rm odd}=0.5is$) or of A_{1g} and A_{2g} symmetry (e.g., $\Delta_{\rm even}=s_{|x^2-y^2|}$, $\Delta_{\rm odd}=s_{xy(x^2-y^2)}$) are found compatible with the Raman data, band-structure calculations, and with corner-superconducting quantum interference device and *c*-axis tunneling results. [S0163-1829(96)03626-0]

Electronic Raman scattering in high-T_c superconductors[1–6] and its theoretical foundations of charge density fluctuations near the Fermi level,[7] low frequency gap formation,[8,9] light induced pair-breaking and polarization dependent gap anisotropies in the superconducting state has not yielded a consensus on the pairing symmetry.[10,11] Electronic Raman scattering probes the electronic structure factor, i.e., the spectrum of electronic excitations near the Fermi level, and directly displays the condensation of low frequency charge density fluctuations below the gap and increased quasiparticle scattering above the gap in the superconducting state. The coupling of the incident and scattered Raman photons to the normal and superconducting electronic system is given by the Raman vertex, i.e., the effective mass tensor contracted by incident and scattered polarization vectors, and can be expressed using $k*p$ perturbation theory.[9] Polarization dependent Raman efficiencies are then determined by the averages of the corresponding effective mass fluctuations over the Fermi surface which has multiple sheets in $YBa_2Cu_3O_{7-\delta}$ (Y-123).[12–14] Screening affects the low frequency density fluctuations which carry a net charge and leads to suppression of the corresponding fully symmetric (A_{1g}) mass fluctuations and the formation of a peak at the plasma frequency. Similar to intervalley scattering in semiconductors, however, unscreened A_{1g} scattering (i.e., corresponding to fluctuations of zero net charge) is observable from multicomponent carrier systems, e.g., multisheeted Fermi surfaces, where nonvanishing differences to the average mass fluctuations exist.[12,13,15–19]

Effective masses and polarization dependent Raman vertices have been recently determined from band-structure calculations. For the normal state electronic Raman continua, effective mass averages over the Fermi surface derived from the local-density-approximation (LDA) band structure[20] of Y-123 yield essentially correct absolute efficiencies in all polarizations thus supporting the validity of *ab initio* band-structure calculations and establishing their relevance in electronic Raman investigations.[21] For the superconducting state, the anisotropies of the superconducting gap and screening effects together with the anisotropic masses determine the frequency and polarization dependence of the spectra and their intensity in the $q\rightarrow 0$ limit. The Fermi surface of Y-123 has four sheets corresponding to the even and odd symmetry $pd\sigma$ states of the CuO_2 planes, the $pd\sigma$ bands of the linear chains, and the $pd\pi$ bands of the apical oxygens.[22] In addition to different masses on each Fermi surface the gaps and respective anisotropies may also be different on each sheet. Even though Raman scattering is not sensitive to the phase of the superconducting order parameter the mass fluctuations yield clearly distinctive gap excitation spectra for different gap sizes and anisotropies. In the following systematic investigation of the Raman spectra of superconductivity induced electronic excitations, the generalized masses and mass fluctuations consistent with the LDA band structure and experimental photoemission results are determined. Then, using the gauge invariant and screening inclusive theory of Abrikosov *et al.*[8] and Klein *et al.*,[9] gap excitation spectra are calculated for a wide range of gap structures and the compatible ones determined in comparison with the experimental results.

High quality single-domain Y-123 crystals ($T_c=91$ K) were either produced by uniaxial stress detwinning or small ones selected as grown by identification in a polarization microscope and their single-domain structure verified by x-ray diffraction. The Raman spectra were taken in a single monochromator-filter spectrograph with a Mepsicron array detector for high sensitivity (incident power <20 W/cm^2), sufficient resolution, and coverage of the normal state continuum to eliminate the possibility of a luminescence background.

Figure 1 shows a set of *a-b* plane polarized and depolarized spectra. The main results are the following: Above 1000 cm^{-1} Raman shift the spectra display the flat continuum attributed to the collision limited response of the normal state. Below 200–500 cm^{-1}, depending on polarization, gaps open up with the redistributed spectral weight shifted to pair-breaking peaks at higher frequencies. In $x+y,x-y$ polarization the pair-breaking peak appears above 650 cm^{-1} while all others peak at about half that frequency. The inten-

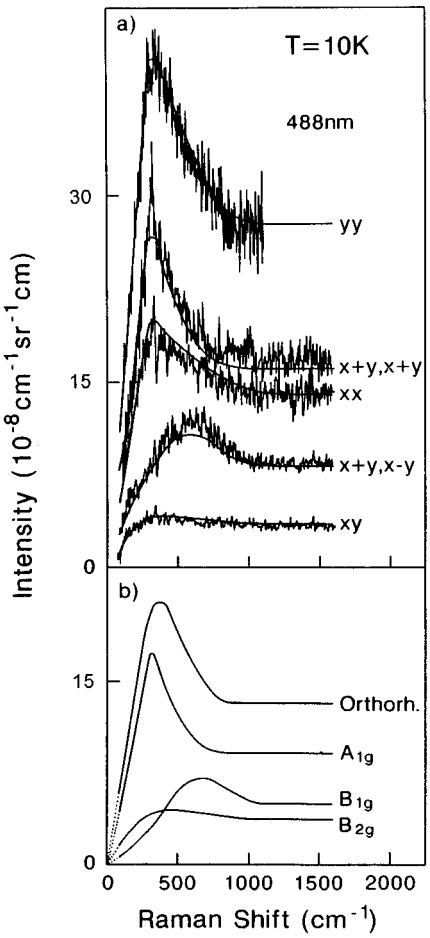

FIG. 1. Polarization dependent 10 K electronic Raman efficiencies of a $YBa_2Cu_3O_{7-\delta}$ single-domain crystal in absolute units (a). Phonons have been subtracted and the spectra normalized to the flat normal state continua. (b) shows frequency dependent Raman tensors of A_{1g}, B_{1g}, B_{2g}, and orthorhombic symmetry, i.e., ($^a\ _a$), ($^b\ _{-b}$), ($^c\ _c$), and ($^0\ _e$), determined by fits to the five spectra of (a) as indicated by the solid lines.

sities of the parallel polarizations dominate. The strong yy and xx polarized spectra display essentially the same behavior except for their large intensity difference attributed to the linear chains and their associated Fermi surface sheet. This justifies analysis in tetragonal Raman tensors of A_{1g} ($^a\ _a$), B_{1g} ($^b\ _{-b}$), and B_{2g} ($^c\ _c$) symmetry augmented by a tensor of ($^0\ _e$) symmetry to account for the chain-induced orthorhombicity. These four frequency dependent tensors were determined from the five spectra and are shown in Fig. 1(b). A_{2g} ($_d\ ^{-d}$) contributions, which may arise from polarization dependent resonances, were found to be small ($<0.5\ B_{2g}$) (Ref. 21) and were omitted from the following discussion. The corresponding fitted spectra agree well with the data as shown by the solid lines in Fig. 1(a) thus justifying the procedure. Even though the scattering intensity observed below 1000 cm^{-1} must be a mixture originating from superconducting and normal state electrons, their separation is difficult to estimate in particular if impurities are present. However, the superconductivity induced intensities above the baselines defined by the respective high frequency normal state continua ($\omega > 1000$ cm^{-1}) can unambiguously be attributed to pair-breaking scattering. Their peak positions, linewidths, and intensities are summarized in Table I, whereby the intensities were determined from the peak areas above their respective $\omega > 1000$ cm^{-1} baselines [Fig. 1(b)].

Calculations of the quasiparticle spectra in the limit $q \to 0$ were made following Klein *et al.*[9] The spectral density describing the superconducting gap excitations is given by

$$\frac{d^2S}{d\omega\, d\Omega} = r_0^2 \hbar N(E_F)\omega^{-1} m^2 \mathrm{Im}\left[\langle \mu^{-2}\lambda\rangle - \frac{\langle \mu^{-1}\lambda\rangle^2}{\langle\lambda\rangle}\right] \quad (1)$$

with

$$\lambda = \frac{4|\Delta|^2}{\sqrt{4|\Delta|^2 - \omega^2}}. \quad (2)$$

Here Δ denotes the k-dependent gap function on the Fermi surface, μ^{-1} the Raman vertex, and $\langle\ \rangle$ the Fermi surface average[9] which includes density of states and geometric correction factors. The Raman vertex is given by the inverse effective mass tensor contracted with incident and scattered polarization vectors $\hat{\mathbf{e}}_L$ and $\hat{\mathbf{e}}_S$ and describes the electronic charge density fluctuations that modulate the plasma polarizability and their strong polarization dependence within and between the different Fermi surface sheets. In a superconductor, this term is weighed by the pair response function which in (2) accounts for the gap structure

TABLE I. Peak positions, linewidths, absolute and normalized integrated Raman efficiencies of the superconductivity-induced electronic Raman response above the normal state continuum baseline [$\omega > 1000$ cm^{-1}, Fig. 1(b)] for A_{1g} ($^a\ _a$), B_{1g} ($^b\ _{-b}$), B_{2g} ($_c\ ^c$), and orthorhombic ($^0\ _e$) symmetry in units of (10^{-6} cm^{-1} sr^{-1}). The data (accuracy $\pm$ 30%) include corrections for optical constants. The ratios of their integrated intensities to the normal state continua are also given together with the respective theoretical estimates based on the plane-only LDA mass fluctuations and the gap structure of [Fig. 5(g)]. The normalized $A_{1g}/B_{1g}/B_{2g}$ intensity ratios of the $A_{1g}-A_{2g}$ gap structure
(Fig. 6) are 0.7/1/0.2 .

	Experiment					Calculations	
Symmetry	Peak (cm^{-1})	FWHM (cm^{-1})	Intensity (10^{-6} cm^{-1}sr^{-1})	Intensity (Normalized)	SC/normal (cm^{-1})	SC/normal (cm^{-1})	Intensity (Normalized)
A_{1g}	310±50	240±100	20	2.7	210	104	0.8
B_{1g}	670±50	400±100	7.5	1	140	139	1
B_{2g}	400±100	450±200	3.9	0.5	100	100	0.3
Orth.	350±50	320±100	28	3.7	220	-	-

and introduces pair-breaking peaks at the $\omega=2\Delta$ singularity. In principle, vertices for all permutations of electron and hole generations on the same and different Fermi surface sheets must be considered.[23] However, for the realistic Fermi surface derived from band-structure calculations, vertices with electron and hole generation on different sheets do not fall in the $q\rightarrow 0$ limit thus making them Raman forbidden. Vertex corrections, which lead to gauge invariance, as well as Coulomb corrections, which account for screening effects of the fully symmetric A_{1g} fluctuations, are included[9] for $q\rightarrow 0$ by subtraction of the second term in (1). Final state interaction leading to quasiparticle lifetime broadening[24] is accounted for by a damping term in (2) taken to be frequency dependent for better agreement with the experimental results.[25] Impurities and collisions can significantly alter the low frequency behavior and linewidths of the pair-breaking peaks.[26,27] Thus the following discussion is limited to pair-breaking peak positions and intensities.

Intensities integrated from the superconductivity induced peaks in the spectra essentially follow the cross sections of the normal state continua in all symmetries as indicated by the ratios (Table I). After establishing their role for the normal state[21] this result confirms the role of the mass fluctuations also for the superconductivity induced electronic Raman vertex. Only gap structures other than isotropic *s* pairing may introduce differences in intensity ratios between superconductivity induced and normal state continua and factors of less than 2 were found for the *s*- and *d*-pairing combinations investigated below. Absolute superconductivity induced intensities calculated for isotropic equally sized *s* gaps were found to be about 1 order of magnitude too low which is similar to deviations found for the normal state continua[21] and may originate from the resonant Laser excitation or lifting of momentum conservation due to collisions permitting Raman vertices between different sheets of the Fermi surface.[12] The A_{1g}, B_{1g}, and *orthorhombic* pair-breaking–normal-intensity ratios are enhanced over the B_{2g} value. This may be a result of the mass fluctuations of the orthorhombic chain Fermi surface [Fig. 1(b)] which, similar to A_{1g}, displays a low frequency pair-breaking peak and gap, is consistent with lower A_{1g} superconducting-normal ratios observed in Bi-2212 and Tl-2223,[28] and the ones calculated without chains below.

Calculations of the mass fluctuations were performed as follows. Essentially all experimental results are contained in the tetragonal A_{1g}, B_{1g}, and B_{2g} spectra, the chain spectra being similar to A_{1g}. Thus it suffices to use the downfolded LDA band-structure results of Andersen *et al.* including only the tetragonal $pd\sigma$ orbitals of the CuO_2 planes.[20] They are consistent with ARPES and dHvA data, have the effect of the chains ($pd\sigma$ orbitals) and the apical oxygens ($pd\pi$ orbitals) properly removed from the band structure and reduce the four-sheeted orthorhombic Fermi surface of Y-123 to two sheets with even and odd symmetry. Only *s*- and *d*-wave gap functions and linear combinations thereof are considered initially. As $|\Delta|^2$ entering in (2) has A_{1g} symmetry, gap structures are only distinguishable by size and anisotropy. Thus it suffices to calculate effective masses of A_{1g}, B_{1g}, and B_{2g} symmetry, i.e., $0.5(\mu_{xx}^{-1}+\mu_{yy}^{-1})$, $0.5(\mu_{xx}^{-1}-\mu_{yy}^{-1})$, and μ_{xy}^{-1} at both Fermi surfaces the results of which are shown in Fig. 2. Here the CuO_2 plane-only

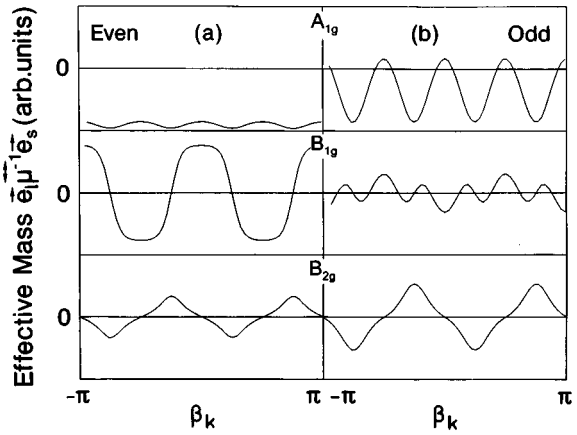

FIG. 2. Effective mass tensors contracted with polarization vectors for the *even* and *odd* Fermi surfaces of the LDA band-structure four-band model in polar coordinates about the *S* point. The results are given in the symmetric irreducible representations of D_4 tetragonal symmetry, i.e., $A_{1g}0.5(\mu_{xx}^{-1}+\mu_{yy}^{-1})$, $B_{1g}0.5(\mu_{xx}^{-1}-\mu_{yy}^{-1})$, and $B_{2g}\mu_{xy}^{-1}$.

four-band model was used and plane dimpling,[20] the low order polynomial approximation of which leads to unrealistic masses, was not included. The masses are not very sensitive to changes in the Fermi level. Only the A_{1g} masses show nonzero averages, a symmetry property, which leads to screening of the corresponding charge fluctuation averages.

To investigate the effects of saddle points and parameter sensitivity, the masses of non-*k*-periodic polynomial type potentials, i.e., $(-a)(x^4+y^4)+b(x^8+y^8)-c(x^4y^4)$ (denoted 4-8-4), were calculated for Fermi levels near their saddle points with *x* and *y* (different from Ref. 20) corresponding to $(1-k_x)$ and $(1-k_y)$, respectively, and $a,b,c>0$. The potentials display saddle points defining a lower limit for the Fermi levels in the models. Even and odd CuO_2 plane Fermi surfaces were simulated by offsetting the Fermi levels and extended saddle points by larger exponents (e.g., 6-12-6). The polynomial potentials are in qualitative agreement with the ARPES and LDA band-structure results, i.e., they produce concentric rounded square Fermi surfaces about the *S* point in the Brillouin zone, saddle points, extended or not at the *X* and *Y* points, and minima at the Γ point. Altogether masses similar to the ones of the four-band model (Fig. 2) for the even and odd Fermi surface sheets were found. This indicates that the presence of saddle points has a limited effect and that the four-band model masses are indeed a result of the band structure and not numerical artifacts of the analytic model[20] at the Fermi level. The main properties of the four-band model masses (Fig. 2) are π periodicity (in polar coordinates about *S*), larger magnitudes of the A_{1g} and B_{1g} but smaller B_{2g} masses of the even compared to the odd Fermi surface, and highly anisotropic A_{1g} and B_{1g} masses of the odd Fermi surface, the topological origin of which may be its proximity to the saddle points which causes a reversal of curvature between (100) and (110) directions. The nodes of the even B_{1g} and B_{2g} masses are defined by symmetry. Mass enhancements were found to be small by comparison of LDA band dispersion and ARPES data.[29] Strong correlation effects have been shown not to introduce effective mass

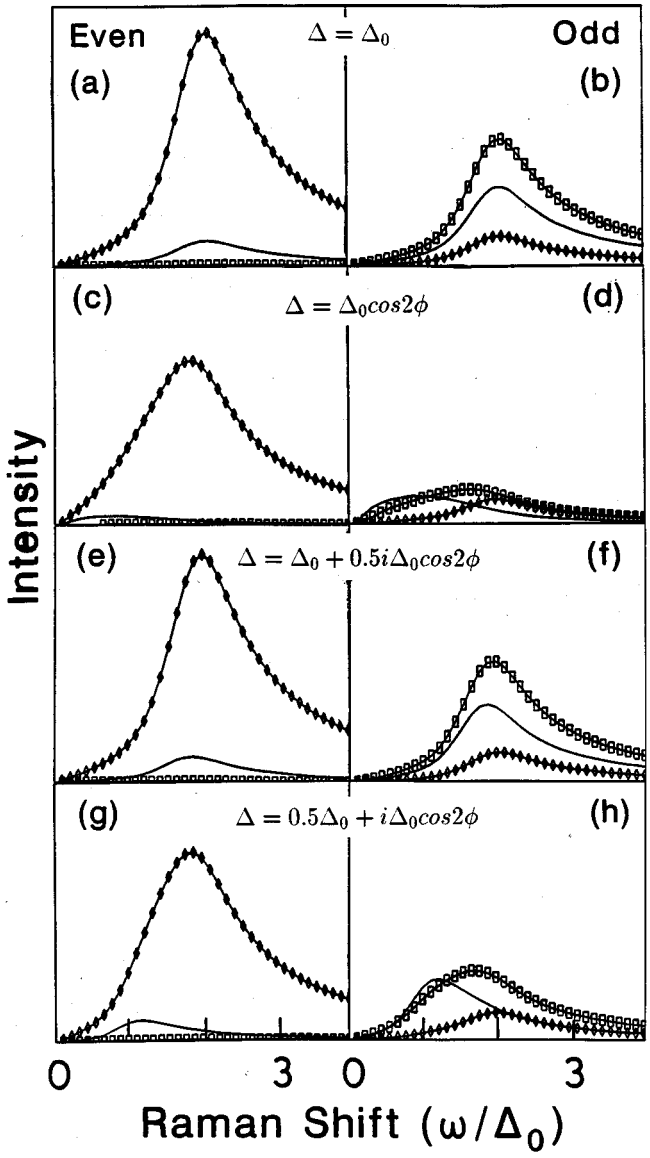

FIG. 3. Superconductivity induced electronic Raman spectra of A_{1g} (rectangles), B_{1g} (diamonds), and B_{2g} symmetry calculated using the mass fluctuations for the single *even* or *odd* Fermi surface sheets of Fig. 2 and s, d, $s+0.5id$, and $0.5s+id$ gaps. Low-energy gap onsets are broadened by damping (Ref. 25) adjusted to represent the data.

anisotropy for different symmetries in heavy fermion systems and similarly are not considered relevant to the conclusions of this paper. Thus the LDA masses of Fig. 2 are considered to be representative of Y-123 at the current state of available and reliable experimental and numerical detail and are used as the basis for the following discussion about gap symmetries compatible with the observed Raman gap excitations.

The square root singularity in (1), which emphasizes contributions at $\omega=2\Delta$, will almost always produce a peak at the maximum gap, i.e., $2\Delta_0$, unless it is suppressed by screening. Recalling the main experimental result of A_{1g}, B_{1g}, and B_{2g} pair-breaking peaks at Raman shifts of Δ_0, $2\Delta_0$, and Δ_0 and intensities ratios of about 4:2:1, respectively, the essential problem in view of the Coulomb screening of A_{1g} symmetry excitations then remains the explanation of the strong low frequency A_{1g} peak with a single gap function. The second term in Eq. (1), which describes screening, will vanish if λ/μ does not contain A_{1g}. For constant masses scattering of A_{1g} symmetry will be screened out. However, unscreened A_{1g} gap excitations are possible to the extent that the anisotropic masses are correlated with an anisotropic gap.

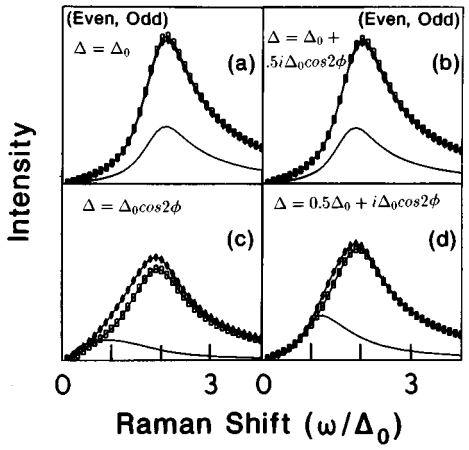

FIG. 4. Superconductivity induced electronic Raman spectra of A_{1g} (rectangles), B_{1g} (diamonds), and B_{2g} symmetry calculated using the mass fluctuations for both *even* and *odd* Fermi surfaces (Fig. 2) with *equal* s, d, $s+0.5id$, and $0.5s+id$ gaps on each sheet including broadening (Ref. 25).

In order to systematically investigate the spectra resulting from multiple Fermi surface sheets with different mass and gap anisotropies, single Fermi surface sheets were evaluated first. Figures 3(a), 3(c), 3(e), and 3(g) show A_{1g}, B_{1g}, and B_{2g} spectra for the masses of the even Fermi surface using isotropic $s-$, $d-$, $s+0.5id$, and $d+0.5is$ gap functions where d denotes $\cos2\phi$ and is indistinguishable from $|\cos2\phi|$ in (2). The B_{1g} spectra, where mass and gap maxima coincide, produce strong peaks at $2\Delta_0$ with larger linewidths in the d-gap cases while the response of the nearly constant A_{1g} mass is completely screened out. The B_{2g} spectra also peak at $2\Delta_0$ in the s-gap dominated cases [Figs. 3(a) and 3(e)], however, when d or anisotropic s gaps dominate [Figs. 5(c) and 5(g)] mass maxima at odd and gap maxima at even multiples of $\pi/4$ lead to weak low frequency B_{2g} pair-breaking peaks. This has been unjustifiedly taken as proof for d-wave pairing, however, other compatible gap symmetries also exist. The spectra of the odd Fermi surface [Figs. 3(b), 3(d), 3(f), and 3(h)] yield strong unscreened A_{1g} peaks at $2\Delta_0$ as a result of highly anisotropic A_{1g} masses. The weaker odd Fermi surface B_{1g} peaks at $2\Delta_0$ are a result of the smaller B_{1g} masses. Thus the mass fluctuations of a single Fermi surface in conjunction with s, d, or anisotropic s gaps always produce B_{1g} pair-breaking peaks at the maximum gap $2\Delta_0$. The A_{1g} peak is either completely screened out or its unscreened remainder for highly anisotropic masses appears near $2\Delta_0$. A significant low frequency shift of the A_{1g} peak from $2\Delta_0$ is only possible with unrealistic A_{1g} masses and at the expense of intensity [e.g., Figs. 3(f) and 3(h)]. It is therefore concluded that the recent d-wave claim,[10] which was based on a single Fermi surface sheet, is not well founded for optimally doped Y-123.

Even and odd Fermi surface mass fluctuations with the same gaps on each sheet are investigated yielding the spectra shown in Fig. 4. As the A_{1g} masses on both sheets are different, unscreened A_{1g} mass fluctuations result in all cases and lead to strong peaks at $2\Delta_0$. For the inherently unscreened mass fluctuations (vanishing mass averages) of B_{1g} and B_{2g} symmetry, the spectra are the superposition of the ones from the individual sheets, whereas the strong unscreened A_{1g} spectra are produced largely from mass fluctuations between different sheets. As a result the experimentally observed strong unscreened A_{1g} intensities are ascribed to intersheet fluctuations between Fermi surfaces with different masses (independent of the peak positions). The A_{1g} peaks at $2\Delta_0$ are caused by the square root singularity in (1) which draws the largest intensity to the gap maximum unless the A_{1g} mass deviations from the multisheeted average exactly vanish in their vicinity. The probability of this occurrence is very small in view of similar low frequency A_{1g} results observed in Tl-2223 and Bi-2212.[28]

Thus it must be concluded that different gap sizes with or without anisotropy are required on both Fermi surface sheets to obtain agreement with the data. Figure 5 shows the results of calculations of (1) with various combinations of s, d, and anisotropic s gaps different on the even and odd Fermi surface sheets. Figures 5(a) and 5(b) display the effect of different sized s gaps. The unscreened A_{1g} peaks are drawn to the maximum deviations from the total A_{1g} mass average which occur on the odd Fermi surface at 0, $\pm\pi/2$, $\pm\pi$ (Fig. 2) while the small even Fermi surface A_{1g} deviation from the average is largely screened out. The B_{1g} and B_{2g} spectra in Figs. 5(a) and 5(b) directly reflect the superposition of the different mass sizes and gaps. The results of different d gaps, shown in Figs. 5(c) and 5(d), yield similar results as in Figs. 5(a) and 5(b) except for the intensity differences and the inherently low B_{2g} frequencies discussed above. Figures 5(e) and 5(f) show the results of a large s gap and a small d-like gap in both possible combinations. The low frequency A_{1g} peak of Figs. 5(a) and 5(c) is now shifted to higher frequencies [Fig. 5(e)] reflecting the effect of the d gap on the odd A_{1g} masses and the Fermi surface averages. Except for intensity differences Fig. 5(f) is almost identical to Fig. 5(b). Figures 5(g) and 5(h) detail the results of a large d gap with a small s gap. With the small s gap on the odd Fermi surface and the d gap on the even sheet the A_{1g} peak appears at low frequency and acquires considerable strength comparable to B_{1g} while the weak B_{2g} peak appears near $1\Delta_0$. Thus except for the low A_{1g} intensity this gap structure agrees quite well with the experimental Raman data. Using this gap structure in conjunction with a 4-8-4 potential correct peak positions and intensities could be produced. Particularly, agreement with experiment is better with this gap structure than in the case of different sized d gaps [Fig. 5(c)], where the B_{2g} frequency is significantly lower than observed and the A_{1g} intensity is smaller.

Summarizing the results of Figs. 5(a)–5(h) consistency with A_{1g}, B_{1g}, and B_{2g} experimental peak positions requires the gap on the odd Fermi surface to be significantly smaller than on the even Fermi surface. The experimental intensities are best reproduced when the gap on the odd Fermi surface is isotropic and the even gap is highly anisotropic. In Figs. 5(i)–5(p) the question of sensitivity of the spectra to different degrees of gap anisotropy and the possible distinction of anisotropic s-wave and d-wave gaps is addressed. Figures 5(i)–5(l) in comparison to 5(c), 5(d), 5(g), and 5(h) show the effects of small d admixture to the s gaps while Figs. 5(m)–5(p) in comparison to Figs. 5(c), 5(d), 5(g), and 5(h) detail the differences of highly anisotropic s gaps versus d gaps. In addition all respective spectra were recalculated using $\cos^2(2\phi)$ gap functions for $\cos(2\phi)$ (not shown). All these results show that peak positions and intensities in the spectra do not change strongly with small differences in the anisotropy of the gaps [e.g., Fig. 5(g) versus 5(m)]. Particularly the Raman detection of nodes in the gap,[30] i.e., a necessary condition for d-wave pairing, appears to be an overinterpretation of the data.[27] Due to the presence of impurities and lifetime effects, which can produce subgap Raman intensities, the claim of gap nodes based on nonvanishing low frequency B_{2g} intensities alone is questionable. This is independent of the number of Fermi surface sheets as their contributions add in the absence of screening.

Gap symmetries for translationally invariant singlet pairing in tetragonal (D_{4h} symmetry) crystals have been identified using group theoretical methods and aid in the determination of compatible gap structures.[31–33] They are the five even parity irreducible representations of the D_{4h} point group, i.e., A_{1g}, A_{2g}, B_{1g}, B_{2g}, and E_g with basis functions $S^+=x^2+y^2$, $S^-=xy(x^2-y^2)$, $D^+=x^2-y^2$, $D^-=xy$, and $E=z(x\pm iy)$, respectively. Thus in principle gaps expandable in five sets of harmonics that transform like the basis functions are allowed including different gaps on different Fermi surface sheets. The irreducible representations for s and anisotropic s pairing are the same while the one for $d_{x^2-y^2}$ pairing is different. Thus s and anisotropic s pairing are not separable on symmetry grounds and will likely be mixed while s and d pairing may be separable by a perturbation of lower symmetry. Without requiring time reversal symmetry, mixed gaps, i.e., $\Delta_1+e^{i\phi}\Delta_2$, with the relative phase as dynamical variable become allowed in addition to the pure symmetries. The relative phase of $\pi/2$ between order parameters of different irreducible representations is favored in this case as it minimizes the free energy in the Ginzburg-Landau expansion.[34] However, for different gaps on different Fermi surfaces completely separated in k space, no states with mixed gaps are expected to exist. In this case the Ginzburg-Landau expansion is not expected to yield a preference for the relative phase of the gaps. Investigating (1) it should be noted that all gaps enter as $|\Delta|^2$. Thus the Fermi surface average will not permit detection of phase effects between Fermi surface sheets and nonsuperconducting sheets will not contribute. If mixed gaps are present on the same sheet, phase shifts are detectable in principle. In the case of $s+id$ versus anisotropic s_1+s_2 pairing, however, the s_1s_2 term in (1) will only produce a slight change in the Raman spectra. Calculations using the gap parameters similar to Figs. 5(i)–5(p) with and without phase differences showed that these effects will hardly be detectable in electronic Raman experiments.

Further insight may be gained by comparing Raman compatible gap symmetries to results of phase sensitive superconducting quantum interference device (SQUID) measurements.[35,36] Corner SNS SQUID results between a Y-123 and a Pb superconductor indicate the presence of a

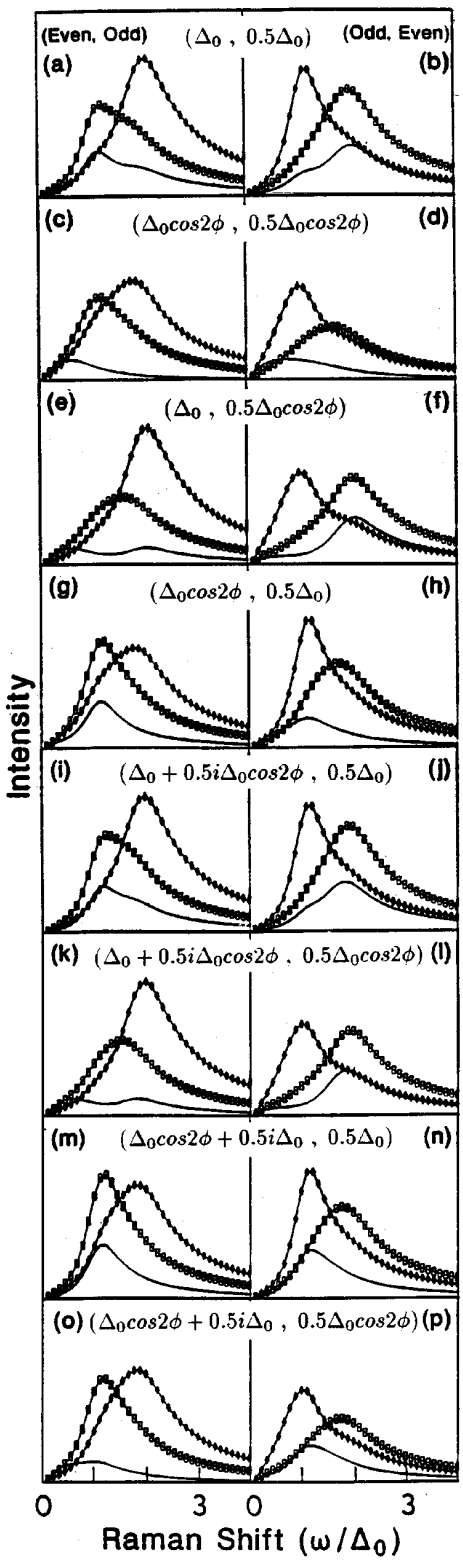

FIG. 5. Superconductivity induced electronic Raman spectra calculated using the mass fluctuations of the *even* and *odd* Fermi surfaces (Fig. 2) with *different* gap sizes and anisotropies on both sheets. A_{1g}, B_{1g}, and B_{2g} spectra are labeled as in Fig. 3 and the *even* and *odd* gaps are exchanged between the left and right figures. Broadening adjusted to represent the data was included.

sign change of the order parameter in the *a-b* plane.[35] However, the finite central minimum value of the critical current at zero flux, the large flux period of the current minima of the corner junction compared to the edge junction, and the *c*-axis tunneling results[36] appear to disagree with the *d*-wave model. The ($\Delta_{\rm even}=d$, $\Delta_{\rm odd}=0.5is$) gap structure compatible with the Raman results [Fig. 5(g)] with the *d* gap on the even and the small *s* gap on the odd Fermi surface indicates somewhat better agreement with the *a-b* plane and *c*-axis SQUID data. Calculations of the expected corner junction critical current versus flux behavior for the ($\Delta_{\rm even}=d$, $\Delta_{\rm odd}=0.5is$) gap structure, whereby equal coupling strengths of the even and odd Fermi surfaces of Y-123 to the Pb Fermi surface were assumed,[37] yield the observed nonvanishing central current minimum but marginal flux period and linewidth consistency with the data.[35] For tunneling in the *c* direction the coupling of the *s* gap on the odd Fermi surface of Y-123 to the Pb Fermi surface reproduces the *c*-axis SQUID data,[36] while the *d* gap yields no net tunneling current.

However, better agreement is produced by the gap structure of $A_{1g}+A_{2g}$ symmetry (both real[38]) shown on the right side of Fig. 6(a). A_{1g} and A_{2g} gaps on the even and odd Fermi surfaces, respectively, are compatible with the Raman data [Fig. 6(b)] and produce agreement with the SNS SQUID data [Fig. 6(c)]. Simulations of corner SQUID tunnel junctions between an $A_{1g}+A_{2g}$ and an A_{1g} superconductor also yield minima of the critical current at vanishing flux through the junction, i.e., periods of two small and one large maxima which, if smoothed, account very well for the observed nonvanishing central minimum and the linewidths.[35] Furthermore, the doubled flux period of consecutive flux minima of the A_{2g} gap compared to the B_{1g} ($d_{x^2-y^2}$) gap may account for the extensive ($6\times$) corner-edge period ratio[35] ($1\times$ is expected for lengths $l_{\rm corner}=2*l_{\rm edge}$ and $d_{x^2-y^2}$ pairing). Changing the external current adjustable phase also yields similar asymmetries as observed[35] for the corner junctions. The *c*-axis SQUID data of Ref. 36 are reproduced by the even Fermi surface A_{1g} gap coupling to the Pb Fermi surface and do not require coupling of the odd Fermi surface, necessary in the $B_{1g}+A_{1g}$ ($\Delta_{\rm even}=d$, $\Delta_{\rm odd}=0.5is$) gap structure, as *c*-axis tunneling from the A_{2g} gap is expected to vanish by symmetry. For clear *k* separation between A_{1g} and A_{2g} gaps (even-odd Fermi surface pairing prohibited in ground state) time reversal symmetry is not expected to be broken consistent with observations[43] and the $\Delta_{A_{1g}}{}^{*}\Delta_{A_{2g}}$ term in the Ginzburg-Landau expansion is expected to vanish. It has been suggested that A_{2g} pairing is promoted by third-neighbor in-plane interaction or antiferromagnetic exchange.[31] Antiferromagnetic spin fluctuations[39] have been argued to favor anisotropic *s* pairing[40] and, for even-odd band splitting, a sign reversal of the gap between the even and odd Fermi surfaces over *d*-wave pairing.[41] However, the suggested complete phase reversal between even and odd Fermi surfaces[41] appears incompatible with the SQUID data and only compatible with the Raman data if different gap sizes are assumed. Kuboki *et al.*[42] have suggested the formation of different gaps ($\Delta_{\pm}=\Delta_{||}\pm\Delta_{\perp}$) on the even and odd Fermi surfaces of the bilayer systems due to interplane interaction. Even though their multiple order parameter model

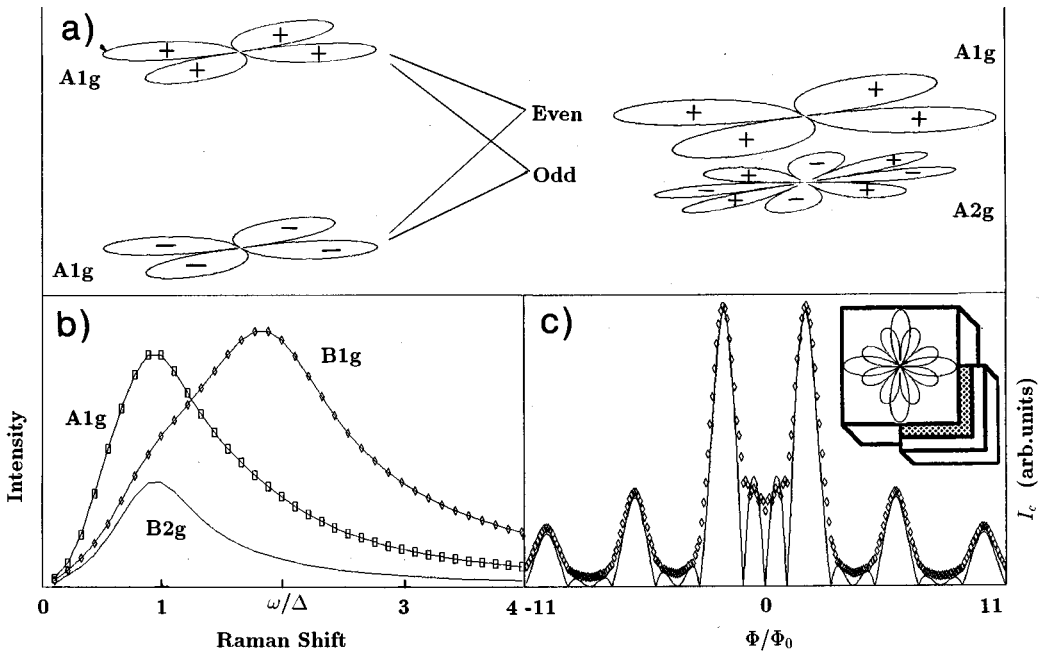

FIG. 6. Calculated Raman (b) and tunneling (c) data of the $A_{1g} + A_{2g}$ gap structure, i.e., $\Delta_{\text{even}} = s_{|x^2-y^2|}$ and $\Delta_{\text{odd}} = s_{xy(x^2-y^2)}$, displayed in (a) in planar k space and vertical real space. (c) shows the calculated and smoothed (diamonds) behavior of the critical current vs flux through the tunnel junction of a SNS corner SQUID between dual gap A_{1g}/A_{2g} and single gap A_{1g} superconductors assuming equal coupling of the A_{1g} and A_{2g} gap Fermi surfaces to the A_{1g} gap Fermi surface of the low temperature superconductor. Even and odd superposition (Ref. 42) of anisotropic A_{1g} single plane gaps augmented to include hybridization for the odd Fermi surface A_{2g} gap is speculated to produce the Raman and SQUID data compatible A_{1g} and A_{2g} symmetry gaps on the *even* and *odd* Fermi surfaces (a).

appears to favor different gap sizes on the even and odd Fermi surfaces, the formation of Raman compatible B_{1g} and A_{1g} symmetry (e.g., $\Delta_{\text{even}} = d_{x^2-y^2}$, $\Delta_{\text{odd}} = 0.5is$) or A_{1g} and A_{2g} symmetry (e.g., $\Delta_{\text{even}} = s_{|x^2-y^2|}$, $\Delta_{\text{odd}} = s_{xy(x^2-y^2)}$) gaps in their model would require $\Delta_{||}$ and $\Delta_{\perp}$ gaps of *equal* size [nontetragonal in case of $\Delta_{A_{1g}}$ and $\Delta_{A_{2g}}$ (Ref. 44)] which appears to contradict expectations of *different* in-plane and interplane interactions. It is thus speculated that an A_{1g} and A_{2g} symmetry gap could result from the even and odd superposition of anisotropic s gaps and hybridization [Fig. 6(a)] of the multiple order parameters into a single time reversal invariant order parameter for each Fermi surface. However, a detailed investigation including model calculations has to be deferred to a later publication. In addition other experimental results also suggest the existence of a dual gap in bilayer cuprates.[45,46]

In summary, absolute superconductivity induced Raman efficiencies of Y-123 have been measured in a-b plane polarizations. The spectral and intensity anisotropies are quantitatively compared with the pair-breaking excitation spectra calculated using effective mass fluctuations from realistic band structures for a wide range of D_{4h} symmetry compatible gaps. It is found that two gaps of different size and anisotropy are required on the CuO_2 plane Fermi surface sheets of even and odd parity. Respective gap structures of B_{1g} and A_{1g} symmetry (e.g., $\Delta_{\text{even}} = d_{x^2-y^2}$, $\Delta_{\text{odd}} = 0.5is$) and A_{1g} and A_{2g} symmetry (e.g., $\Delta_{\text{even}} = s_{|x^2-y^2|}$, $\Delta_{\text{odd}} = s_{xy(x^2-y^2)}$) are identified. They are compatible with the Raman data as shown by calculated Raman spectra based on the mass fluctuations of the band structure, the corner- and c-axis SQUID tunneling data and preserve time inversion symmetry due to complete k separation.

Numerous discussions with M. Cardona on the electronic Raman effect, O.K. Andersen, I.I. Mazin, and A.I. Liechtenstein on the LDA band structure, and verification of the normal state Raman efficiencies by S. Donovan are gratefully acknowledged.

[1] A.V. Bazhenov *et al.*, in *Novel Superconductivity*, edited by S.A. Wolff and V.S. Kresin (Plenum Press, New York, 1987), p. 893.
[2] K.B. Lyons, S.H. Liou, M. Hong, H.S. Chen, J. Kwo, and Y.T. Negran , Phys. Rev. B **36**, 5592 (1987).
[3] S.L. Cooper, M.V. Klein, B.G. Pazol, J.P. Rice, and D.M. Ginsburg, Phys. Rev. B **37**, 5920 (1988).
[4] A. Yamanaka, T. Kimura, F. Minami, K. Inoue, and S. Takekawa, Jpn. J. Appl. Phys. **27**, L1902 (1988).
[5] R. Hackl, W. Gläser, P. Müller, D. Einzel, and K. Andres, Phys. Rev. B **38**, 7133 (1988).
[6] M.C. Krantz, H.J. Rosen, J.Y.T. Wei, and D.E. Morris, Phys. Rev. B **40**, 2635 (1989); M.C. Krantz, J. Phys. Chem. Solids **54**, 1331 (1993).
[7] A. Zawadowski and M. Cardona, Phys. Rev. B **42**, 10 732 (1990).
[8] A.A. Abrikosov and V.M. Genkin, Sov. Phys. JETP **38**, 417 (1974).

[9] M.V. Klein and S.B. Dierker, Phys. Rev. B **29**, 4976 (1984).
[10] T.P. Devereaux *et al.*, Phys. Rev. Lett. **72**, 396 (1994); **72**, 3291 (1994).
[11] M. Krantz and M. Cardona, Phys. Rev. Lett. **72**, 3290 (1994).
[12] I. Ipatova, A.V. Subashiev, and V.A. Voitenko, Solid State Commun. **37**, 893 (1981).
[13] M. Cardona and I.P. Ipatova, in *Elementary Excitations in Solids*, edited by J.L. Birman, C. Sebenne, and R.F. Wallis (Elsevier, Amsterdam, 1992), p. 237.
[14] M. Krantz and M. Cardona, J. Low Temp. Phys. **99**, 205 (1995).
[15] N. Mestres and M. Cardona, Phys. Rev. Lett. **55**, 1132 (1985).
[16] G. Contreras, A.K. Sood, and M. Cardona, Phys. Rev. B **32**, 930 (1985); **32**, 924 (1985); F. Cerdeira, N. Mestres, and M. Cardona, *ibid.* **29**, 3737 (1984).
[17] P.M. Platzman, Phys. Rev. A **139**, 379 (1965); P.M. Platzman and P.A. Wolff, *Waves and Interactions in Solid State Plasmas* (Academic Press, New York, 1973).
[18] M. Chandrasekhar, M. Cardona, and E.O. Kane, Phys. Rev. B **16**, 3579 (1977).
[19] G. Abstreiter, M. Cardona, and A. Pinczuk, in *Light Scattering in Solids IV*, edited by M. Cardona and G. Güntherodt (Springer, Berlin, 1984), Chap. 1.
[20] O.K. Andersen, O. Jepsen, A.I. Liechtenstein, and I.I. Mazin, Phys. Rev. B **49**, 4145 (1994).
[21] M.C. Krantz, I.I. Mazin, D.H. Leach, W.Y. Lee, and M. Cardona, Phys. Rev. B **51**, 5949 (1995).
[22] O.K. Andersen, A.I. Liechtenstein, C.O. Rodriguez, I.I. Mazin, O. Jepsen, V.P. Antropov, O. Gunnarson, and S. Gopalan, Physica C **185-189**, 147 (1991).
[23] A. Zawadowski (private communication).
[24] A. Zawadowski and M. Cardona, Phys. Rev. B **42**, 10 732 (1990).
[25] Damping and the singularity in Eq. (2) was numerically accounted for by substituting $\Delta^2 \rightarrow \Delta^2 + i\epsilon\omega^2$ with $\epsilon = 0.1$ and using the unrestricted Fermi surface average of Ref. 9. Except for minor differences introduced by the damping, which was adjusted to correspond to the broad peaks observed in the data, use of the Tsuneto function [Eq. (9) of 9] and the finite temperature formalism [Eqs. (6d) and (28d) of 9] for $q = 0$ yields the same results.
[26] T.P. Devereaux, Phys. Rev. B **45**, 12 965 (1992).
[27] M.C. Krantz (unpublished).
[28] M.C. Krantz *et al.* (unpublished).
[29] J.C. Campuzano, G. Jennings, A.J. Arko, R.S. List, B.W. Veal, and R. Benedek, J. Phys. Chem. Solids **52**, 1411 (1991).
[30] X.K. Chen, J.C. Irwin, H.J. Trodahl, T. Kimura, and K. Kishio, Phys. Rev. Lett. **73**, 3290 (1994).
[31] F. Wenger and S. Östlund, Phys. Rev. B **47**, 5977 (1993).
[32] M. Sigrist and T.M. Rice, Z. Phys. B. **68**, 9 (1987).
[33] M. Sigrist and K. Ueda, Rev. Mod. Phys. **63**, 239 (1991).
[34] G. Koitlar, Phys. Rev. B **37**, 3664 (1988).
[35] D.A. Wollman, D.J. Van Harlingen, J. Giapintzakis, and D.M. Ginsberg, Phys. Rev. Lett. **74**, 797 (1995).
[36] A.G. Sun, D.A. Gajewski, B.M. Maple, and R.C. Dynes, Phys. Rev. Lett. **72**, 2267 (1994).
[37] While a coupling of the even Fermi surface of Y-123 to the Pb Fermi surface in the tunneling Hamiltonian appears obvious (Ref. 42), an equally strong coupling of the odd Y-123 Fermi surface has been included. A possible cause for the coupling of the odd Fermi surface may be an assumed interfacial lattice mismatch, which is expected to produce unit cell doubling or multiplying in the *c* direction in the Pb superconductor leading to even-odd band splitting near the interface. Furthermore, the density of states on the odd Fermi surface of Y-123 being 2.4 times greater than on the even Fermi surface (Ref. 21) favors tunneling involving the odd band. Other interfacial effects facilitating the conversion of the tunneling quasiparticles to eigenstates of the other host crystal in unconventional superconductors have been covered by Sigrist *et al.* (Ref. 33), namely spin flips induced by differences in spin orbit coupling on either side of the junction and local parity breakdown leading to coupling of even and odd parity gaps.
[38] For complete *k* separation of the even and odd Fermi surface no mixed gap states, which would promote a $\pi/2$ phase shift between gaps, are expected to be present. In addition, a term in the Ginzburg-Landau free energy, which couples to orthorhombic strain (Ref. 42), may produce a vanishing phase shift.
[39] P. Monthoux and D. Pines, Phys. Rev. B **49**, 4261 (1994).
[40] S. Chakravarty, A. Sudbo, P.W. Anderson, and S. Strong, Science **261**, 337 (1993); A. Sudbo *et al.*, Phys. Rev. B **49**, 12 245 (1994).
[41] A.I. Liechtenstein, I.I. Mazin, and O.K. Andersen, Phys. Rev. Lett. **74**, 2303 (1995).
[42] K. Kuboki and P.A. Lee, J. Phys. Soc. Jpn. **64**, 3179 (1995).
[43] A. Mathai, Y. Gim, R.C. Black, A. Amar, and F.C. Wellstood, J. Superconduct. **8**, 491 (1995); see also M. U. Ubbens and P. A. Lee, Phys. Rev. B **50**, 438 (1994).
[44] The possibility of spontaneous breaking of the lattice symmetry associated with the transition to the superconducting state has already been pointed out in Ref. 42.
[45] N. Klein, N. Tellmann, H. Schulz, K. Urban, S.A. Wolf, and V.Z. Kresin, Phys. Rev. Lett. **71**, 3355 (1993).
[46] G.T. Jeong *et al.*, Phys. Rev. B **49**, 15 416 (1994).